Inhibition of GSK-3 Induces Differentiation and Impaired Glucose Metabolism in Renal Cancer

Krishnendu Pal[1], Ying Cao[1], Irina N. Gaisina[3], Santanu Bhattacharya[1], Shamit K. Dutta[1], Enfeng Wang[1], Hendra Gunosewoyo[3], Alan P. Kozikowski[3], Daniel D. Billadeau[1,2], and Debabrata Mukhopadhyay[1]

Abstract

Glycogen synthase kinase-3 (GSK-3), a constitutively active serine/threonine kinase, is a key regulator of numerous cellular processes ranging from glycogen metabolism to cell-cycle regulation and proliferation. Consistent with its involvement in many pathways, it has also been implicated in the pathogenesis of various human diseases, including type II diabetes, Alzheimer disease, bipolar disorder, inflammation, and cancer. Consequently, it is recognized as an attractive target for the development of new drugs. In the present study, we investigated the effect of both pharmacologic and genetic inhibition of GSK-3 in two different renal cancer cell lines. We have shown potent antiproliferative activity of 9-ING-41, a maleimide-based GSK-3 inhibitor. The antiproliferative activity is most likely caused by G_0–G_1 and G_2–M phase arrest as evident from cell-cycle analysis. We have established that inhibition of GSK-3 imparted a differentiated phenotype in renal cancer cells. We have also shown that GSK-3 inhibition induced autophagy, likely as a result of imbalanced energy homeostasis caused by impaired glucose metabolism. In addition, we have demonstrated the antitumor activity of 9-ING-41 in two different subcutaneous xenograft renal cell carcinoma tumor models. To our knowledge, this is the first report describing autophagy induction due to GSK-3 inhibition in renal cancer cells. *Mol Cancer Ther; 13(2); 285–96. ©2013 AACR.*

Introduction

Renal cell carcinoma (RCC), the most common malignant neoplasm arising from the kidney, accounts for approximately 3% of all human cancers. It is the sixth most common cancer in men and eighth most in women. Every year, an estimated 65,000 people in the United States are diagnosed with RCC, and approximately 13,500 patients succumb to RCC-related disease (1). Furthermore, about one third of patients with RCC have already developed metastatic progression at initial diagnosis and up to one half of patients develop distant metastases after primary tumor resection (2). The 5-year survival rate for patients with metastatic RCC is less than 10% due to acquired resistance of tumors to chemotherapy and radiotherapy. Immunotherapy failed to significantly improve survival as its efficacy was less than 20% (3). Recent advances in molecular targeting have pro-

duced several tyrosine kinase inhibitors (TKI) sunitinib, pazopanib and sorafenib, mTOR inhibitors, and anti-VEGF–humanized antibody bevacizumab as the first- and second-line treatment of systemic therapy for RCC (4–7). However, the treatment response is not long-standing and TKI treatment poses risks of serious adverse events (8).

Various factors contribute to RCC progression and metastasis, NF-κB being one of them (9–11). Previous studies suggested a definitive role of glycogen synthase kinase-β (GSK-3β) in the regulation of NF-κB activity (12–14). GSK-3, a serine/threonine protein kinase, was originally discovered as a protein kinase that phosphorylates and inactivates glycogen synthase (GS), an enzyme involved in glycogen biosynthesis (15, 16). There are two distinct GSK-3 family members, GSK-3α and GSK-3β (17), which share more than 98% sequence homology within their kinase domains; only GSK-3α has an extended N-terminal glycine-rich tail (18). Although both isoforms have shared substrates, they exhibit different expression patterns, substrate preferences, and cellular functions (12, 19).

Unlike most protein kinases, GSK-3 is constitutively active in normal conditions and undergoes a rapid and transient inhibition in response to a number of external signals (20). GSK-3 plays important roles in numerous signaling pathways that regulate a variety of cellular processes (21–25). Because of these diverse roles, malfunction of this kinase is also known to be involved in the pathogenesis of human diseases such as diabetes, inflammation, neurologic disorders, and various neoplastic

Authors' Affiliations: Departments of [1]Biochemistry and Molecular Biology and [2]Immunology, Mayo Clinic College of Medicine, Rochester, Minnesota; [3]Department of Medicinal Chemistry and Pharmacognosy, University of Illinois at Chicago, Chicago, Illinois

Corresponding Author: Debabrata Mukhopadhyay, Mayo Clinic College of Medicine, 200 First Street SW, Guggenheim 1321C, Rochester, MN 55905. Phone: 507-538-3581; Fax: 507-293-1058; E-mail: mukhopadhyay.debabrata@mayo.edu

American Association for Cancer Research

diseases (18, 26). Therefore, GSK-3 is recognized as an attractive target for the development of new drugs.

Several GSK-3 inhibitors have been identified as therapeutic agents in Alzheimer disease, neurodegenerative disorders, and bipolar disorder (27). Recent studies have shown that GSK-3 inhibitors induce growth suppression and apoptosis in human chronic lymphocytic leukemia (14), glioma (28), colon cancer (29), renal cancer (30), and breast cancer (31). In addition, several maleimide-based GSK-3 inhibitors have been shown to elicit excellent antiproliferative activity in pancreatic (32) and ovarian (33) cancer cells.

In the present study, we analyzed the antiproliferative effect of both pharmacolgic and genetic inhibition of GSK-3 in two different renal cancer cell lines and explored the underlying mechanism. We have shown that $G_0–G_1$ and $G_2–M$ phase arrest is the most likely cause of this antiproliferative effect. We further demonstrated that GSK-3 inhibition induces a differentiation phenotype in the renal cancer cells. We have also described that GSK-3 inhibition creates an imbalance in normal energy homeostasis through impaired glucose metabolism in these renal cancer cells, which compels them to enter autophagy. Most importantly, we have demonstrated the inhibitory effect of 9-ING-41, a maleimide-based GSK-3 inhibitor (32, 33), on tumor growth in two different subcutaneous RCC tumor xenograft models *in vivo*. To our knowledge, this is the first report exploring the mechanism behind autophagy induction due to GSK-3 inhibition in renal cancer cells.

Materials and Methods

Reagents

The antibodies against phospho-GSK-3β, GS, phospho-GS, 5′-Adenosine monophosphate-activated protein kinase-alpha (AMPK-α), phospho-AMPK-α, AMPK-β, phospho-AMPK-β, LC3B, and p21 were purchased from Cell Signaling Technology. Antibodies against phospho-p21, Id-1, and cyclin D were purchased from Santa Cruz Biotechnology. Anti-β-actin and anti-GSK-3β were from BD Biosciences. Anti-Ksp-cadherin antibody was purchased from Abcam. Immunohistochemistry was performed using the IHC Select HRP/DAB Kit from Millipore. The compound 9-ING-41 was synthesized as previously described (32).

Cell culture

786-O (CRL-1932; purchased on November 2006) and A498 (HTB-44; purchased on December 2007) cells were purchased from American Type Culture Collection. No authentication of the cell lines was done by the authors. Cells were maintained in Dulbecco's Modified Eagle Medium (DMEM; Life Technologies) supplemented with 10% FBS (Fisher Scientific) and 1% penicillin–streptomycin (Invitrogen) at 37°C in a humidified atmosphere with 5% CO_2. Cultures of 85% to 90% confluency were used for all of the experiments.

Thymidine incorporation assay

Cells (2×10^4) were seeded in 24-well plates and cultured for 24 hours. After 24 hours, the cells were treated with dimethyl sulfoxide (DMSO) or increasing concentration of 9-ING-41 for 72 hours. During the last 4 hours, 1 μCi of [^{3}H] thymidine was added to each well. Four hours later, cells were washed with chilled PBS, fixed with 100% cold methanol, and collected for measurement of trichloroacetic acid-precipitable radioactivity. Experiments were repeated three times in triplicates.

siRNA-based downregulation experiments

Cells were seeded in 6-cm dishes and cultured for 18 to 24 hours. The next day, cells were washed with OPTI-MEM reduced-serum medium and transfected with 100 nmol/L GSK-3β siRNA (Qiagen; target sequence: 5′-CCCAAATGTCAAACTACCAAA-3′, sense: 5′-CAAAU-GUCAAACUACCAAATT-3′, antisense: 5′-UUUGGUA-GUUUGACAUUUGGG-3′) or Allstar Negative Control siRNA (Qiagen) using DharmaFECT 4 (Thermo Scientific). After 5 hours, antibiotic-free DMEM supplemented with 10% FBS was added and cells were incubated for a total of 72 hours before further processing.

Western blot analysis

Western blot analysis was performed to detect the expression levels of phospho-GSK-3β, GSK-3β, GS, phospho-GS, AMPK-α, phospho-AMPK-α, AMPK-β, phospho-AMPK-β, LC3B, cyclin D, phospho-p21, p21, Ksp-cadherin, Id-1, and β-actin in 786-O and A498 cell lysates. Cells were treated with different doses of 9-ING-41 and incubated for 24 to 48 hours. Whole-cell lysates in radioimmunoprecipitation assay (RIPA) buffer supplemented with protease inhibitor cocktail and with or without phosphatase inhibitor were then prepared. Supernatant was collected by centrifugation at 13,000 rpm for 10 minutes. Subsequently, samples were subjected to SDS-PAGE and then transferred to polyvinyl difluoride membranes and immunoblotted for the proteins of interest. Antibody-reactive bands were detected by enzyme-linked chemiluminescence (Amersham). These experiments were repeated three times.

In vitro apoptosis assay

Cells were seeded in 6-cm dishes and cultured for 18 to 24 hours. The next day, cells were treated with either DMSO or increasing concentrations of 9-ING-41 for 48 hours. Cell surface expression of phosphatidylserine, resulting from apoptosis, was measured using Annexin-V-FITC (Biovision, Mountain View, CA) and a FACScan flow cytometer (Beckton-Dickinson). Additional exposure to propidium iodide (PI) made it possible to differentiate early apoptotic cells (Annexin-positive and PI-negative) from late apoptotic cells (Annexin- and PI-positive). Results are representative of three separate experiments.

Cell-cycle analysis

Cells were treated with either DMSO or increasing concentrations of 9-ING-41 for 24 hours as mentioned earlier. Cells were then harvested by trypsinization and fixed in ice-cold 70% ethanol for 1 hour. The fixed cells were washed twice with PBS and resuspended in a 500 µL aliquot of modified Vindelov's DNA staining solution (10 µg/mL RNase A and 5 µg/mL of PI in PBS). Flow cytometric analysis was done with flow cytometry system (FACScan flow cytometer; Becton-Dickinson). Cells in the G_0–G_1, S, and G_2–M phases of the cell cycle were determined with FCS Express (De Novo Software). Results are representative of three separate experiments.

Intracellular glucose measurement assay

Cells were seeded in 6-cm dishes and cultured for 18 to 24 hours. The next day, cells were treated with either DMSO or increasing concentrations of 9-ING-41 for 24 hours. Cells were then washed with PBS, trypsinized, and centrifuged. The cell pellet was used to measure intracellular glucose using Amplex Red Glucose Assay Kit (Life Technologies) following slight modifications to the manufacturer's protocol. The cell pellet was washed twice in PBS and resuspended in 1X reaction buffer from the kit. While keeping on ice, cells were lysed by probe sonication with three cycles of 10 seconds on and 30 seconds off at 20% power. Fifty microliters of reaction solution (10 mmol/L Amplex Red, 10 U/mL of horseradish peroxidase (HRP), 100 U/mL of glucose oxidase, 50 mmol/L of sodium phosphate buffer, pH 7.4) was added to 50 µL of cell lysate in a 96-well microtitre plate and incubated in the dark at 37°C for 30 minutes. The fluorescence (excitation: 544, emission: 590) was then measured using a SpectraMax plate reader. The values were expressed as Relative Fluorescence Units (RFU)/mg protein.

Immunofluorescence study

786-O or A498 cells grown on coverslip were treated with either DMSO or 1 µmol/L 9-ING-41 for 48 hours. Cells were washed with PBS and fixed with 4% paraformaldehyde for 15 minutes at room temperature followed by washing three times with PBS. Cells were then permeabilized with 0.05% Triton-X in PBS for 15 minutes at room temperature, washed in PBS, and blocked for 1 hour at room temperature with 2% bovine serum albumin (BSA) in PBS containing 0.05% Tween-20 (PBS-T). After the blocking step, cells were incubated overnight at 4°C with LC3B antibody in blocking buffer. The next morning, cells were washed three times with PBS-T and incubated with an Alexa-Fluor-568-tagged secondary antibody for 1 hour at room temperature. The cells were then washed twice in PBS-T, once in PBS, and mounted onto slides using Vectashield with DAPI (Vector Labs) mounting medium. Confocal microscopy was performed using a Zeiss LSM 780 confocal laser scan microscope.

Tumor model

Six- to eight-week-old male nude mice were obtained from the NIH and housed in the institutional animal facilities. All animal work was performed under protocols approved by the Mayo Clinic Institutional Animal Care and Use Committee. To establish tumor growth in mice, 5×10^6 786-O or A498 cells, resuspended in 100 µL of PBS, were injected subcutaneously into the left flank.

In vivo antitumor activity

Tumors were allowed to grow for 21 days without treatment, and mice were then randomized into two groups (six animals per group). Group 1 was treated with PBS containing 50% polyethylene glycol (PEG-400) alone, whereas group 2 was treated with 9-ING-41 in the above vehicle at doses of 20 mg/kg three times a week intraperitoneally. After 4 weeks of treatment, all tumor-bearing mice were sacrificed by asphyxiation with CO_2; tumors were removed, weighed, and prepared for immunochemistry. A part of each tumor was homogenized to obtain lysates that were used for Western blot analysis.

Histologic study

Tumors were removed and fixed in neutral buffered 10% formalin at room temperature for 24 hours before embedding in paraffin and sectioning. Sections were deparaffinized and then subjected to hematoxylin and eosin (H&E), Ksp-cadherin, and Ki67 immunochemistry according to the manufacturer's instructions (DAB 150; Millipore). Stable diaminobenzidine was used as a chromogen substrate, and the sections were counterstained with a hematoxylin solution. Photographs of the entire cross-section were digitized using an Olympus camera (DP70). The Ki67-positive nuclei were counted in three different sections. To access heterogeneity with regard to proliferation within an individual tumor, sections were taken from three different areas of the tumor and the proliferative index was determined.

Statistical analysis

The independent-samples t-test was used to test the probability of significant differences between groups. Statistical significance was defined as $P < 0.05$ (*); statistical high significance was defined as $P \leq 0.01$ (**). Error bars are given on the basis of calculated SD values.

Results

ADME/Tox and PK profile of 9-ING-41

We carried out an extensive structure−activity relationship analysis, in vitro pharmacology, and animal studies on a variety of synthesized GSK-3β analogs, which were inspired by the structure of the natural product staurosporine, a hit identified from a small high-throughput screening (HTS) campaign (Fig. 1A). From our library of approximately 100 ATP-competitive GSK-3β inhibitors, the benzofuran-3-yl-(indol-3-yl)maleimide 9-ING-41 has been identified as a potent antiproliferative agent against pancreatic and ovarian cancer cells (32, 33). This compound was previously shown to attenuate tumor
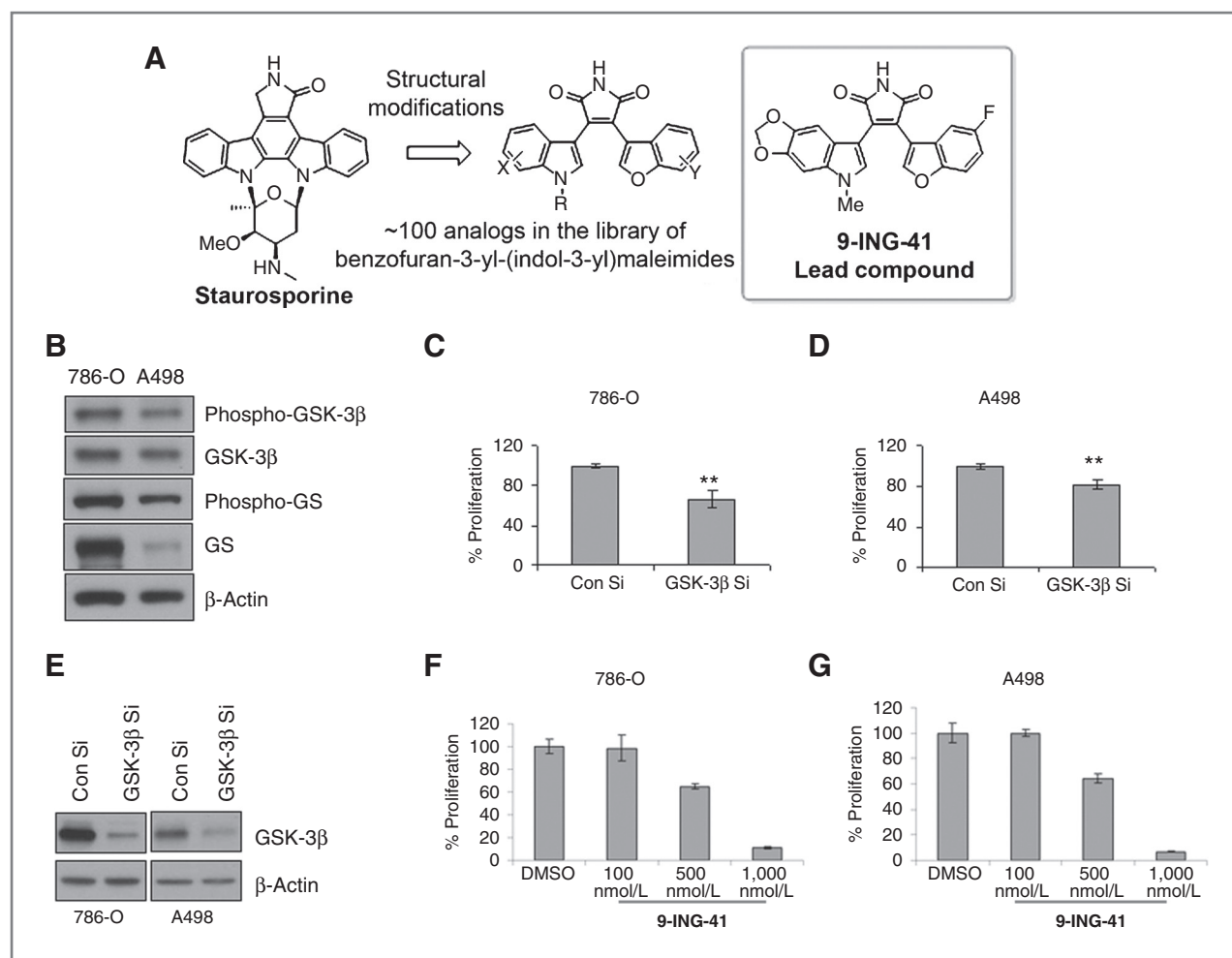
Figure 1. Inhibition of GSK-3 decreases renal cancer cell proliferation *in vitro*. A, chemical structure of 9-ING-41, a maleimide-based GSK-3 inhibitor and its parent compound staurosporine. B, renal cancer cells 786-O and A498 were checked for GSK-3 and GS levels. β-Actin levels served as loading control. C and D, siRNA-mediated downregulation of GSK-3β showed a slight yet significant inhibition of proliferation in both 786-O and A498 cells (**, $P < 0.01$). Proliferation was measured using ^{3}H-thymidine incorporation assay. E, Western blot analysis of siRNA-mediated downregulation of GSK-3β in 786-O and A498 cells. F and G, 786-O and A498 cells were treated with increasing concentrations of 9-ING-41, a novel GSK-3 inhibitor, for 72 hours. The cell proliferation was measured using ^{3}H-thymidine incorporation assay. The figures are representative of three separate experiments (in triplicates) with similar results.

progression *in vivo* in a xenograft model of SKOV3 ovarian cancer growth (33).

In order to obtain the kinase selectivity profile, compound 9-ING-41 was tested at a single dose of 10 μmol/L for kinase inhibition in a panel of 320 kinases (Reaction Biology Corp.). The single dose run was performed in duplicates and the average value was measured. Only 35 kinases were found to have less than 50% remaining activity (Supplementary Table S1). Representative 11 kinases selected from this group were measured for their IC$_{50}$ values ranging from 650 nmol/L to 9,410 nmol/L (Supplementary Table S2). The preliminary ADME/Tox properties of 9-ING-41, including CYP inhibition, metabolic stability, plasma protein binding, and hERG inhibition, were also obtained (Stanford Research Institute International and Cerep, Inc.; Supplementary Table S3). The inhibitory effect on the *in vitro* CYP activity in human liver microsomes was screened using a high-throughput

multiple CYP assay for CYP1A2, CYP2B6, CYP2C9, CYP2C19, CYP2D6, and CYP3A4. In the presence of 10 μmol/L of 9-ING-41, none of the CYP isoforms had activity that was less than 50% of the control, with the exception of CYP3A4 (32% of the control for 9-ING-41), suggesting that this compound is not likely to significantly alter the metabolism of other xenobiotics or endogenous compounds that are substrates for the most common CYP isoforms. This is especially important for putative cancer drugs that will likely be used in combination with other agents. The metabolic stability of 9-ING-41 was studied using human liver microsomes, in which it was found that 78.9% of the parent compound remained after 60 minutes of incubation. The IC$_{50}$ value for hERG inhibition (patch-clamp) by 9-ING-41 was found to be 21 μmol/L, indicating a low potential for cardiac toxicity. Range-finding toxicology studies of 9-ING-41 were carried out in male and female Sprague Dawley rats. The compound

was well tolerated at 500 mg/kg single oral dosage during the toxicity study throughout an 8-day period with no adverse effects observed in body weight, clinical pathology, or gross necropsy findings. Pharmacokinetic analysis of the plasma levels indicated that the volumes of distribution were ≥10 L/kg, suggesting that this compound was well distributed to the tissues and the elimination half-life was 4.85 hours (Supplementary Table S3). Collectively, the compound 9-ING-41 has been demonstrated to possess reasonable PK and ADME/Tox profiles.

GSK-3 inhibition leads to proliferation inhibition in renal cancer cells

We used two renal cancer cell lines, 786-O and A498, which express different levels of GSK-3β and GS for our experiments (Fig. 1B). When GSK-3β was genetically depleted in these two cell lines, there was a small yet significant inhibition in proliferation (Fig. 1C, D, and E).

The effect is slightly more pronounced in 786-O than in A498, which can be explained by a greater abundance of GSK-3β in 786-O cells. When the cells were treated with an ATP-competitive GSK-3 inhibitor, 9-ING-41, a dose-dependent decrease in cell proliferation was observed at both instances (Fig. 1F and G). A 500 nmol/L dose was sufficient for approximately 40% inhibition in proliferation in both the renal cancer cell lines, whereas a 1,000 nmol/L dose resulted in almost complete inhibition of proliferation. Taken together, these findings suggest that GSK-3 plays an important role in cancer cell proliferation.

9-ING-41 induces cell-cycle arrest in renal cancer cells

Given that 9-ING-41 inhibits the proliferation of both 786-O and A498 renal cancer cell lines, we investigated its effect on apoptosis and cell cycle. No significant induction of apoptosis was observed in both cell lines (Fig. 2A).
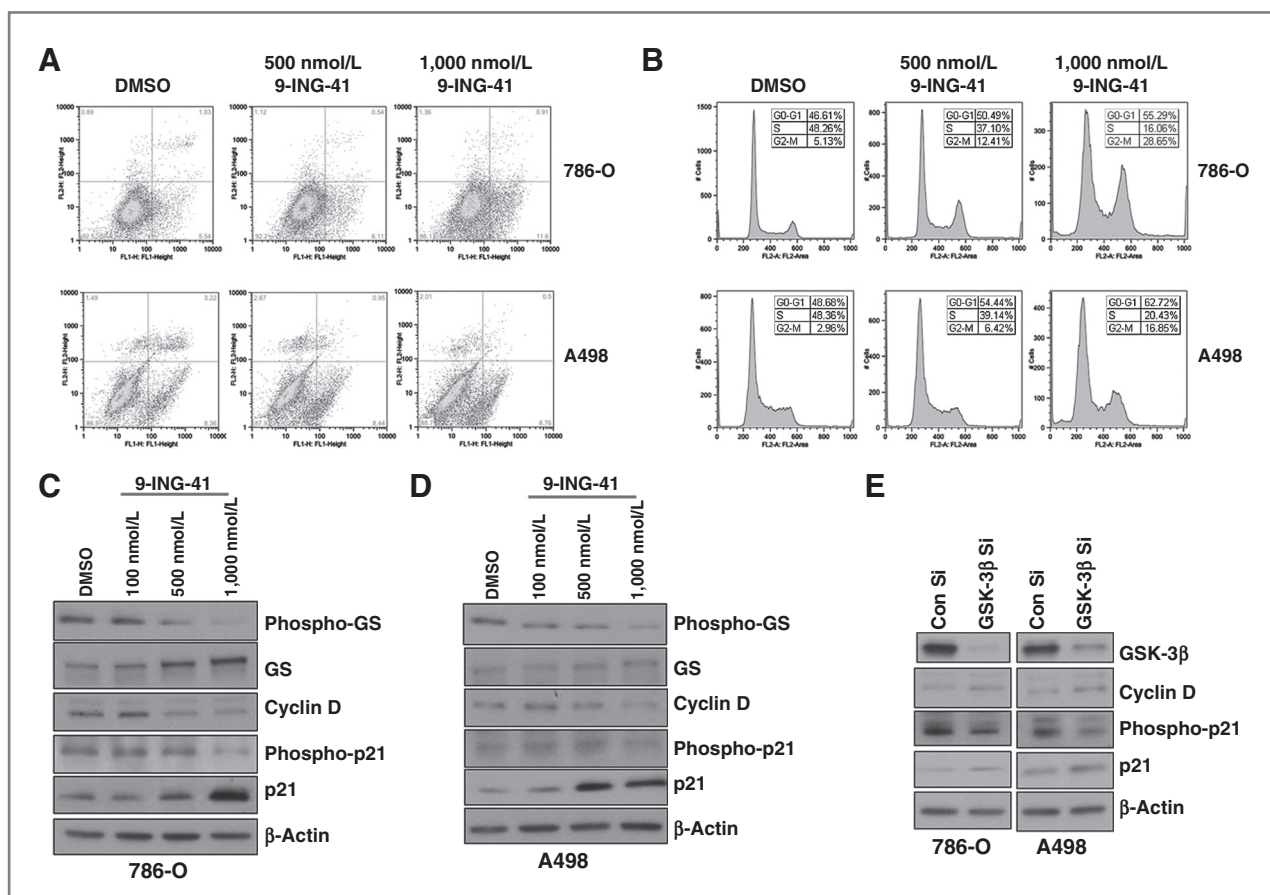

Figure 2. 9-ING-41 induces cell-cycle arrest in renal cancer cells. A, analysis of apoptosis induction property of 9-ING-41 in renal cancer cells by flow cytometry. Cells were treated with increasing concentrations of 9-ING-41 for 48 hours. Apoptosis was measured by Annexin-FITC/PI method. Dead cells (PI-positive) were differentiated from late apoptotic cells (Annexin- and PI-positive), early apoptotic cells (Annexin-positive and PI-negative), and live cells (Annexin- and PI-negative). The figures are representative of three separate experiments with similar results. B, cell-cycle analysis of renal cancer cells treated with increasing doses of 9-ING-41 for 24 hours. DNA content was analyzed by flow cytometry. The figures are representative of three separate experiments with similar results. C and D, 786-O and A498 cells were treated with increasing concentrations of 9-ING-41 for 24 hours. 9-ING-41 inhibits the expression of cyclin D in a dose-dependent manner. In addition, 9-ING-41 inhibits the phosphorylation and consequent degradation of p21, a cyclin-dependent kinase (CDK) inhibitor that directly inhibits the activity of cyclin D/Cdk4/6 complex. β-Actin levels served as loading control. E, similar results were obtained upon siRNA-mediated downregulation of GSK-3β in both the cancer cells. However, cyclin D levels slightly increased here.

However, at 1,000 nmol/L there was a slight increase in the percentage of early apoptotic cells in 786-O (from 5.54% in DMSO-treated group to 11.6% in 1,000 nmol/L 9-ING-41–treated group). In contrast, 9-ING-41 induces cell-cycle arrest in both cell lines. With increasing concentrations of 9-ING-41, the fraction of cells distributed in the S phase decreased significantly compared with cells in other phases (Fig. 2B). In addition, 9-ING-41 downregulated cyclin D1 protein expression in a dose-dependent manner in both cell lines (Fig. 2C and D). It also inhibits the phosphorylation and subsequent degradation of p21, a known substrate of GSK-3β. p21 is a cyclin-dependent kinase inhibitor that directly inhibits the activity of the cyclin D/Cdk4/6 complex, thus inhibiting cell-cycle progression from G_1 to S phase. Genetic depletion of GSK-3β, on the other hand, increased cyclin D1 expression, although inhibition of p21 degradation could still be clearly seen (Fig. 2E). Therefore, the induction of cell-cycle arrest by 9-ING-41 may not be due to GSK-3 inhibition. However, our results indicate that 9-ING-41 suppressed cell proliferation by inducing cell-cycle arrest through a combinatorial effect of downregulation of cyclin D1 expression and inhibition of cyclin D1/Cdk4/6 complex activity.

GSK-3 inhibition induces differentiation in renal cancer cells

Because GSK-3 has been shown to control epithelial–mesenchymal transitions (34–37), we further examined the consequences of 9-ING-41 treatment in 786-O and A498 renal cancer cell lines with respect to differentiation phenotypes under *in vitro* conditions. Upon 9-ING-41 treatment, both cancer cell lines showed a dose-dependent increase in Ksp-cadherin and decreased Id-1 expression (Fig. 3A and B). Genetic depletion of GSK-3β showed similar results (Fig. 3C). Simultaneous treatment of 9-ING-41 and GSK-3β siRNA did not elicit any significant additive or synergistic effect (Fig. 3D and E), which indicates that 9-ING-41 imparts a differentiated phenotype in renal cancer cells through GSK-3 inhibition.
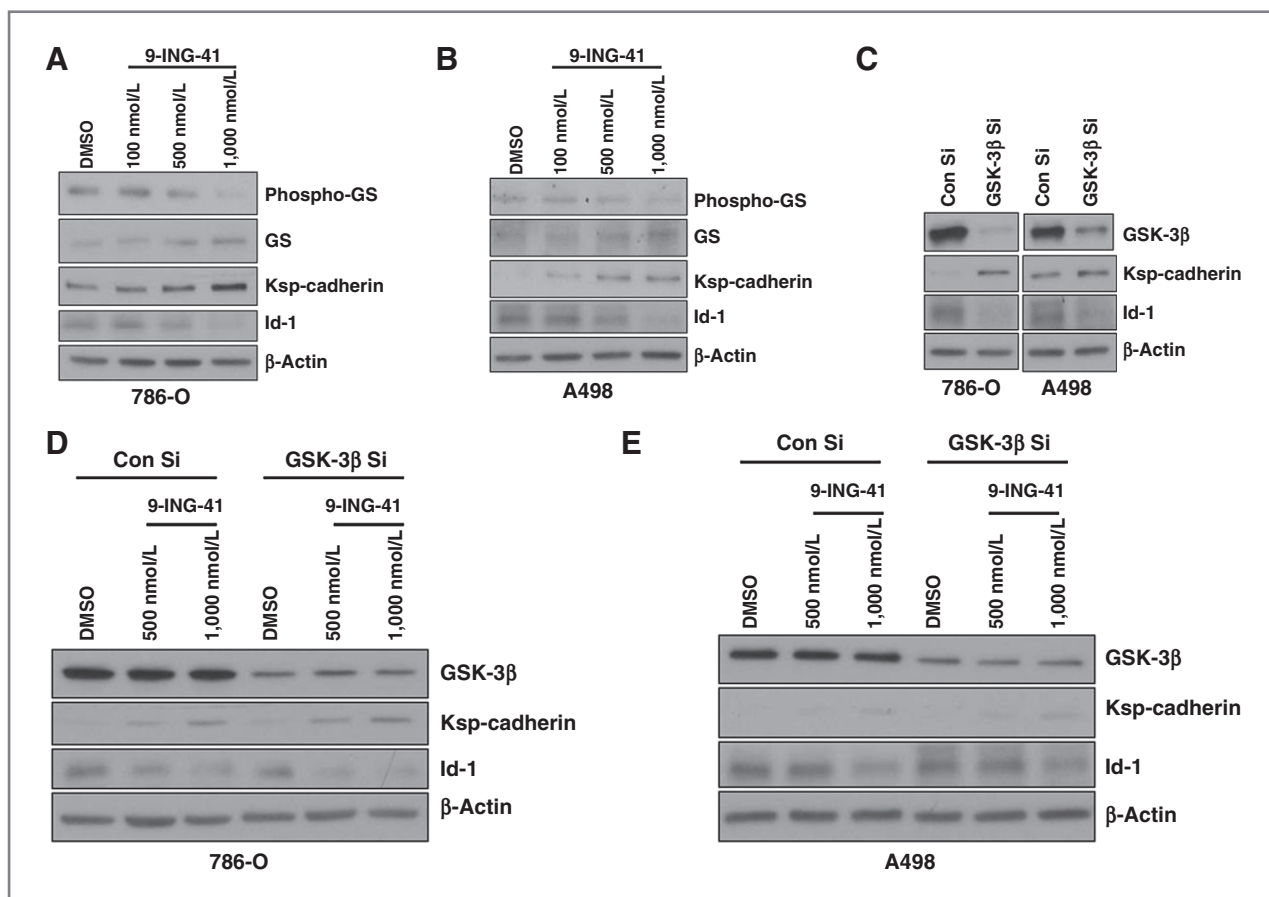
Figure 3. GSK-3 inhibition induces differentiation in renal cancer cells. A and B, 786-O and A498 cells were treated with increasing concentrations of 9-ING-41 for 48 hours. 9-ING-41 induced Ksp-cadherin expression and inhibited Id-1 expression in a dose-dependent manner in both the cancer cells. β-Actin levels served as loading control. C, similar results were obtained upon siRNA-mediated downregulation of GSK-3β in both the cancer cells. D and E, 786-O and A498 cells were simultaneously treated with GSK-3β siRNA and 9-ING-41 to evaluate any additive or synergistic effects on Ksp-cadherin or Id-1 expression.
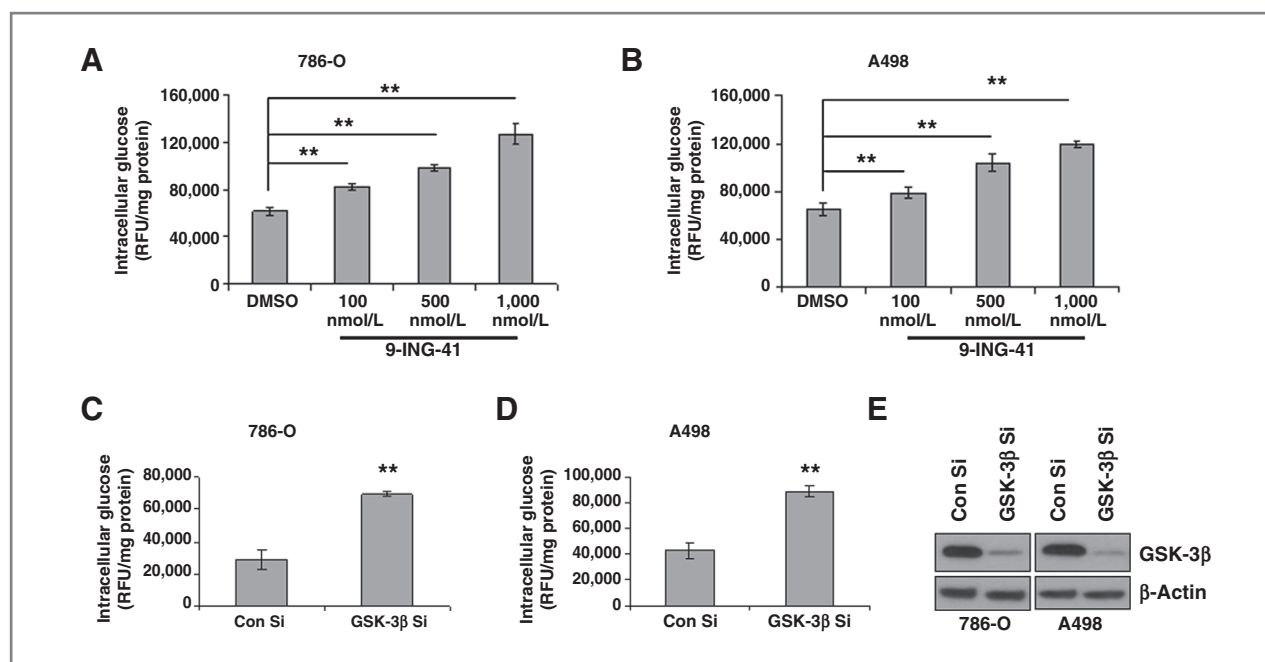
Figure 4. Inhibition of GSK-3 increases intracellular glucose storage. A and B, 786-O and A498 cells were treated with increasing doses of 9-ING-41 for 24 hours. Intracellular glucose storage was measured using the Amplex Red Glucose/Glucose Oxidase Assay Kit as per manufacturer's protocol. The values were expressed as RFU/mg protein. There was a dose-dependent increase in intracellular glucose in both the renal cancer cells. C and D, siRNA-mediated downregulation of GSK-3β also increased intracellular glucose storage in both the cells. The figures are representative of three separate experiments (in triplicates) with similar results. E, Western blot analysis of siRNA-mediated downregulation of GSK-3β in 786-O and A498 cells.

GSK-3 inhibition increases intracellular glucose storage

Because GSK-3 phosphorylates and deactivates GS, inhibition of GSK-3 should result in the activation of GS, ensuing increased glucose storage. Therefore, we chose to analyze the effect of 9-ING-41 on intracellular glucose levels. Not surprisingly, a dose-dependent increase of intracellular glucose was observed in both 786-O and A498 cells upon 9-ING-41 treatment (Fig. 4A and B). Similar results were obtained upon genetic depletion of GSK-3β as well (Fig. 4C, D, and E). These results indicate that GSK-3 regulates the storage of glucose inside the cells.

GSK-3 inhibition affects energy homeostasis and induces autophagy

We then sought to explore whether increased glucose storage had any effect on normal energy homeostasis in renal cancer cells. Upon GSK-3 inhibition with 9-ING-41 treatment, we found an increase in phosphorylation of both AMPK-α and AMPK-β (Fig. 5A and B), suggesting an elevated AMP/ATP ratio that signifies less ATP production and decreased glucose metabolism. Activation of AMPK also repressed mTOR signaling by inhibiting mTOR phosphorylation. Similar results were obtained upon genetic depletion of GSK-3β (Fig. 5C). This observation led us to hypothesize that in order to maintain the energy needed for cellular processes, cells would enter autophagy. This hypothesis was verified through the observation of increased levels of LC3B as ascertained by

both Western blot analysis and immunofluorescence studies (Fig. 5D). These results indicate that GSK-3 has a regulatory role in maintaining cellular energy homeostasis and dysregulation of this pathway will produce metabolic stress in cells.

GSK-3 inhibition inhibits *in vivo* tumor growth

To study the effect of GSK-3 inhibition on renal cancer *in vivo*, we injected 786-O and A498 cells subcutaneously in male nude mice in two separate experiments. Three weeks after tumor inoculation, a 20 mg/kg dose of 9-ING-41 was administered intraperitoneally three times a week. After 4 weeks of treatment, we observed significant reduction of tumor growth in the 9-ING-41–treated group compared with the control group in both tumor models ($P < 0.05$ in both instances). In the 786-O tumor model, the average tumor weight was 517.55 ± 223.85 mg in the control group versus 279.18 ± 91.26 mg in the 9-ING–treated group. In the A498 tumor model, the tumor weights were 609.06 ± 111.8 mg versus 327.4 ± 171.4 mg in the control and treatment groups, respectively (Fig. 6A and B).

We further investigated the effect of GSK-3 inhibition on tumor cell proliferation as measured by Ki67 staining in tumor tissue sections. The abundance of Ki67-positive nuclei was significantly lower in the 9-ING-41–treated group compared with the control group in both 786-O and A498 tumor models (Fig. 6C, D, and E). Significant upregulation of Ksp-cadherin expression was also observed in the 9-ING-41–treated group (Fig. 6C).
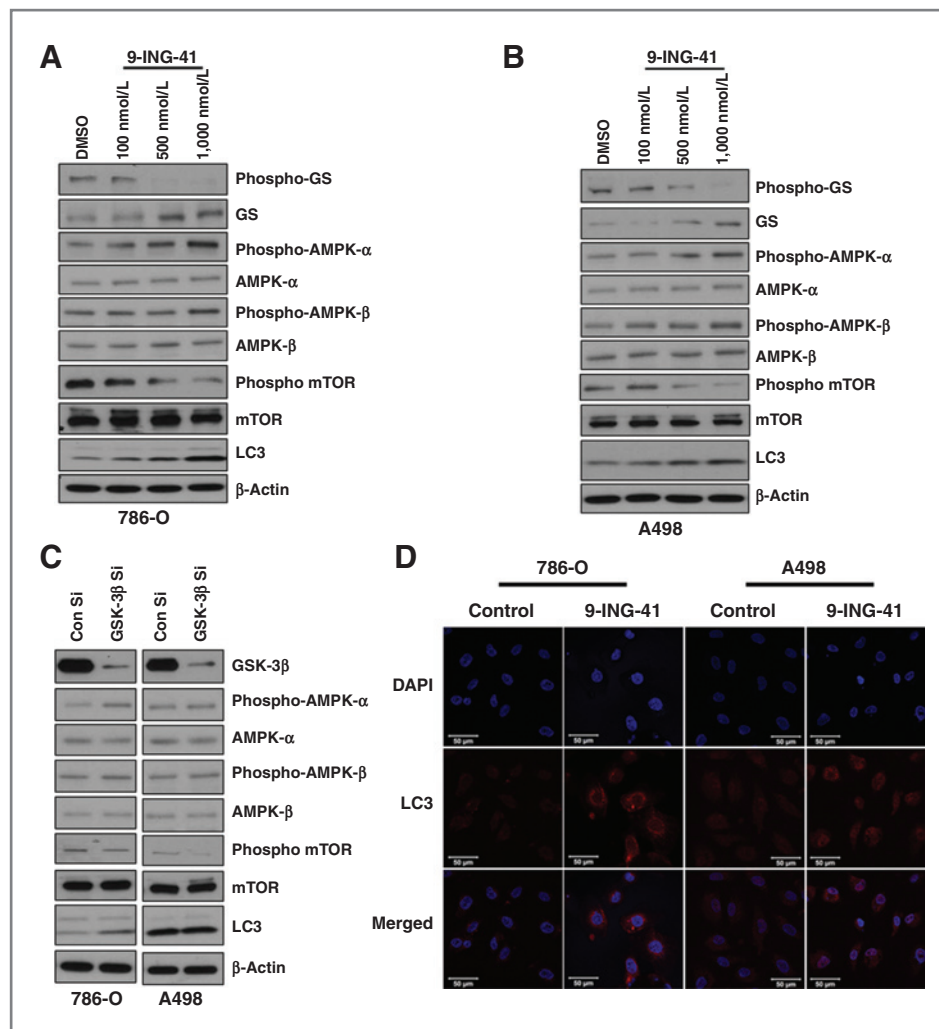
Figure 5. GSK-3 inhibition affects energy homeostasis and induces autophagy. A and B, 786-O and A498 cells were treated with increasing concentrations of 9-ING-41 for 24 to 48 hours. 9-ING-41 induced phosphorylation of both AMPK-α and AMPK-β and inhibited mTOR phosphorylation in both the renal cancer cells. Induction of autophagy was indicated by an increase in LC3 levels. β-Actin levels served as loading control. C, similar results were obtained upon siRNA-mediated downregulation of GSK-3β in both the cancer cells, albeit the effects were slightly less in comparison with 9-ING-41. D, confocal images showing upregulation of LC3 level in 9-ING-41–treated cells. Bar length, 50 μm.

Western blot analysis of lysates prepared from representative tumors of control and treatment group more or less correlated with key *in vitro* results (Fig. 6F and G). These results suggest that GSK-3 regulates *in vivo* proliferation and dedifferentiation in RCC.

Discussion

It is well documented that GSK-3β is overexpressed in RCC cell lines compared with normal kidney cells, and pharmacologic inhibition of GSK-3 suppresses proliferation of renal cancer cells (30). A higher level of phosphorylated GS, a primary GSK-3 substrate, was also observed in RCC cell lines compared with normal kidney, suggesting that GSK-3 is active in RCC. Aberrant nuclear accumulation of GSK-3β was detected in more than 90% human RCC clinical samples and it strongly correlates with phospho-GS expression. This indicates that GSK-3β is active in more than 90% human RCC samples. In contrast, only weak cytoplasmic expression of GSK-3β was found in normal kidney or benign kidney tumors and no phopho-GS was detected in those

tissues indicating GSK-3β inactivity. Interestingly, genetic depletion of GSK-3β, but not GSK-3α, leads to a significant decrease in renal cancer cell proliferation. Previous studies had shown that pharmacologic inhibition of GSK-3 resulted in apoptosis induction through decreased expression of NF-κB target genes Bcl-2 and XIAP in pancreatic cancer (13), chronic lymphocytic leukemia (CLL; ref. 14), and renal cancer (30). It has also been shown that GSK-3β contributes to the maintenance of active chromatin at Bcl-2 and XIAP promoters, allowing p65 binding and transcriptional activation of Bcl-2 and XIAP in cancer cells (14). However, GSK-3 regulates numerous cellular processes involving a number of signaling pathways. Accordingly, the NF-κB pathway may not be solely responsible for the antiproliferative effect exerted by both pharmacologic and genetic inhibition of GSK-3.

Here, we describe the antiproliferative effect of a novel ATP-competitive GSK-3 inhibitor, 9-ING-41, in two different renal cancer cells *in vitro* and *in vivo*. In this study, it has clearly been shown that the pharmacologic inhibition of GSK-3β by treatment of 9-ING-41
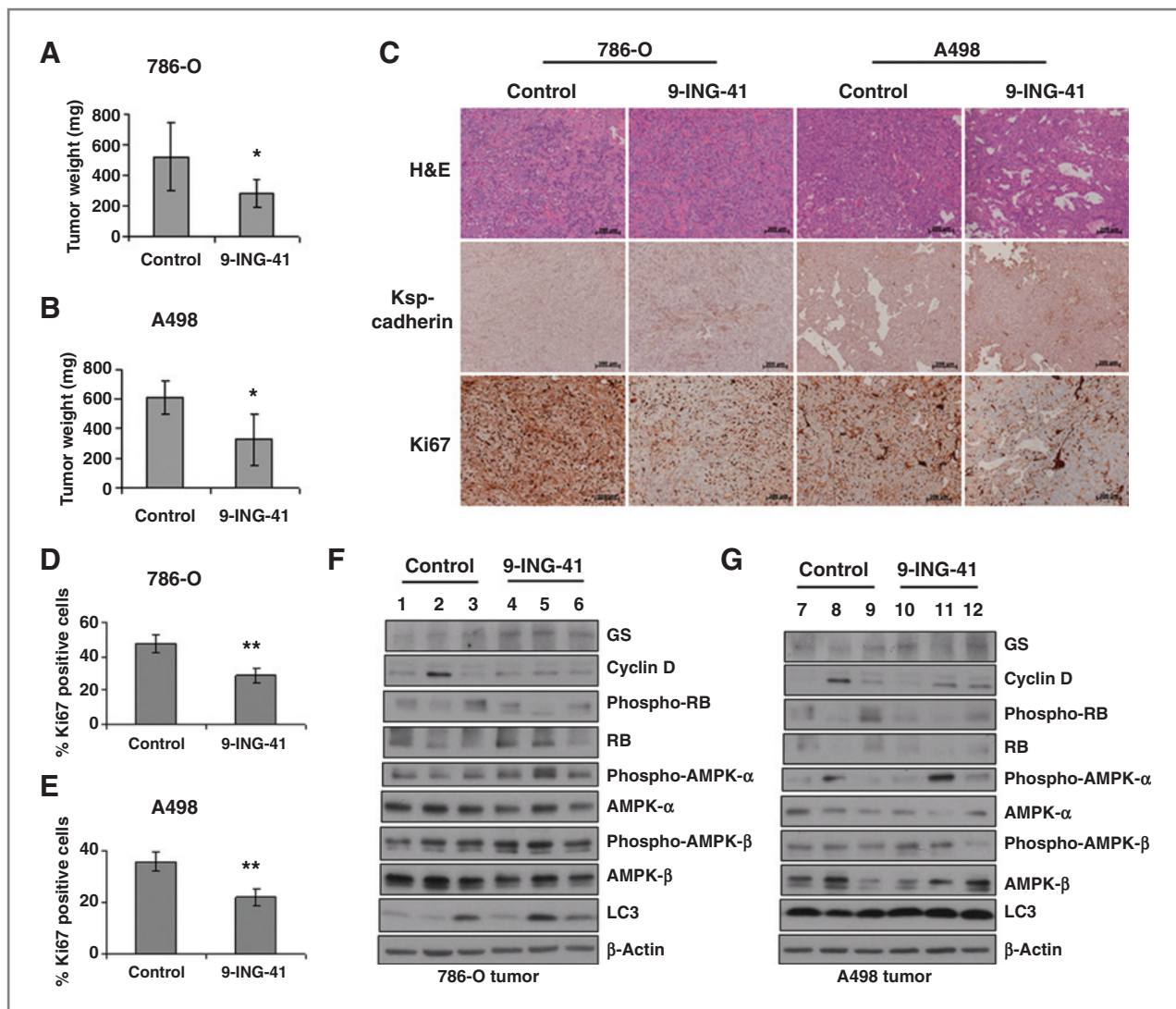
Figure 6. GSK-3 inhibition inhibits tumor growth in nude mice. A and B, in two different experiments, 6- to 8-weeks-old male nude mice received subcutaneous injections of 5×10^6 786-O and A498 cells, respectively. Tumors were allowed to grow for 21 days before the initiation of single-agent treatment with 9-ING-41 (20 mg/kg) in PBS containing 50% PEG-400. The control group received only PBS containing 50% PEG-400. After 4 weeks of treatment, significant reduction in tumor weight was observed in both experiments (*, $P < 0.05$). C, H&E, Ksp-cadherin, and Ki67 immunohistochemical staining in formalin-fixed tissue sections obtained from tumors of control and treatment group. Bar length = 200 μm. D and E, quantification of Ki67-stained nuclei in 786-O and A498 tissue sections, respectively (**, $P < 0.01$). F and G, Western blot analysis with lysates obtained from representative tumor samples of vehicle-treated and 9-ING-41–treated groups to correlate with key in vitro results. RB, retinoblastoma.

caused cell growth inhibition with $IC_{50} < 1$ μmol/L. Genetic depletion of GSK-3β also showed significant inhibition of renal cancer cell proliferation, albeit to a lower extent than 9-ING-41. These observations are in accordance with previous findings (30) and can be explained by the fact that 9-ING-41 cannot discriminate between GSK-3α and GSK-3β and inhibits them equally (Supplementary Table S1).

Because 9-ING-41 inhibited proliferation in the renal cancer cell lines, we decided to analyze its effect on apoptosis induction and cell cycle. We found that 9-ING-41 did not induce apoptosis to a significant extent, but arrests the cells in both G_0–G_1 and G_2–M phases. This

results in less number of cells in the S phase, which explained the reduced proliferation as measured by ^{3}H incorporation. We then checked the expression of two cell cycle regulatory proteins, cyclin D1 and p21, to confirm this. Cyclin D1/Cdk4/6 complex formation is essential for the G_1 to S phase transition, which can be considered as a proliferation index. p21 is a cyclin-dependent kinase inhibitor that directly inhibits the activity of the cyclin D1/Cdk4/6 complex, thereby inhibiting cell-cycle progression. Treatment with 9-ING-41 inhibited cyclin D1 expression as well as phosphorylation and subsequent degradation of p21 in both the renal cancer cell lines tested. A previous study has shown similar results in

which a GSK-3 inhibitor induced cell death through cyclin D1 depletion in breast cancer cells (31). Genetic depletion of GSK-3β, on the other hand, increases cyclin D1 expression. So, it may be possible that the cell-cycle arrest caused by 9-ING-41 may not be due to GSK-3β inhibition; rather some other pathways may be involved. However, it should be noted that the genetic depletion of GSK-3β results in p21 accumulation as well. So, there is a distinct possibility that the activity of the cyclin D1/Cdk4/6 complex will still be diminished causing cell growth inhibition even if there is an increased cyclin D1 expression.

In addition to its antiproliferative effects, 9-ING-41 also imparted a differentiation phenotype to both the renal cancer cell lines tested. A significant increase in Ksp-cadherin level and simultaneous decrease in the Id-1 level were observed upon treatment with 9-ING-41 or genetic depletion of GSK-3β. Simultaneous treatment of 9-ING-41 and GSK-3β siRNA did not show a significant additive or synergistic effect on Ksp-cadherin and Id-1 expression, which indicates that this differentiation phenotype caused by 9-ING-41 treatment is due to GSK-3 inhibition. Ksp-cadherin is a kidney-specific member of the cadherin family found exclusively in epithelial cells of kidney distal tubules and collecting ducts. Its expression is almost undetectable in RCC samples (38). Accordingly, the increase in Ksp-cadherin expression upon GSK-3 inhibition indicates transition from a more tumorigenic mesenchymal state to an epithelial direction. Id-1, on the other hand, has been shown to be frequently upregulated in RCC and its expression levels are positively associated with both tumor grade and stage (39). Therefore, the decrease in Id-1 expression upon GSK-3 inhibition signifies decreased tumorigenicity. Taken together, these data suggest a definitive role of GSK-3 in differentiation and tumorigenicity in renal cancer.

Previous studies reported that GSK-3 plays a role in regulating glucose transport in several cell types and inhibition of GSK-3 resulted in an almost 2-fold increase in glucose uptake (40). Here, we have shown that upon GSK-3 inhibition by 9-ING-41 treatment or genetic depletion of GSK-3β, the intracellular glucose levels increased in both the renal cancer cell lines. However, GSK-3 inhibition also increases GS activity promoting the conversion of cellular glucose into glycogen. Hence, we hypothesized that even if glucose uptake is increased upon GSK-3 inhibition, that glucose cannot be metabolized readily because it is being stored as glycogen, thus creating an imbalance in normal energy homeostasis. This hypothesis is likely true because we show increased phosphorylation of AMPK-α and AMPK-β upon GSK-3 inhibition. Phosphorylation of AMPK repressed mTOR phosphorylation as well. A recent study indicates similar role of GSK-3 in inhibiting AMPK catabolic activity (41). AMPK is phosphorylated (or activated) when the AMP/ATP ratio becomes high which signifies high AMP and low ATP concentration. As ATP is produced during metabolism, a lower ATP concentration signifies a lower rate of metabolism. We also argue that because the cells cannot metabolize the stored glycogen to produce energy required for maintaining cellular processes, autophagy is induced. Autophagy is the degradation of unnecessary or dysfunctional cellular components through the formation of autophagosomes to ensure cellular survival during starvation by maintaining cellular energy levels. Several previous reports show evidence of contrasting effects of GSK-3 in regulating autophagy (42–48). Here, we have shown that GSK-3 inhibition induced autophagy as evident from increased LC3B levels in the renal cancer cells upon GSK-3 inhibition. Because mTOR phosphorylation was inhibited upon GSK-3 inhibition and activation of AMPK acts by repressing mTOR, it is likely that this autophagy induction is mediated through AMPK–mTOR signaling pathway.

Furthermore, it is well established that AMPK activation is inversely correlated with prognosis and survival in RCC (49), and activators of AMPK show potent inhibitory effects on RCC cells (50). Because GSK-3 inhibition increased AMPK activation, this can be used as a therapeutic strategy for the treatment of RCC. In the present study, we have shown the antitumor effect of GSK-3 inhibitor 9-ING-41 in two different subcutaneous xenograft models of RCC in male nude mice. We found that a single-agent treatment with 9-ING-41 caused significant tumor growth inhibition in both 786-O and A498 xenograft models compared with the control group. 9-ING-41 also inhibited *in vivo* tumor cell proliferation as shown by reduction in Ki67 staining. Major *in vitro* results such as GS upregulation, cyclin D1 downregulation, Ksp-cadherin upregulation, AMPK phosphorylation, and LC3 upregulation was validated *in vivo* as well, although inherent heterogeneity of tumors needs to be considered here. We also found that the phosphorylation of retinoblastoma protein decreased in 9-ING-41–treated groups, which signified inhibition of cyclin D1/Cdk4/6 activity.

Taken together, our work uses a maleimide-based GSK-3 inhibitor to elucidate the effect of GSK-3 inhibition on differentiation and energy homeostasis in renal cancer. We have also shown significant tumor growth inhibition in RCC models upon treatment with the aforementioned GSK-3 inhibitor, which may open up further therapeutic strategies for RCC.

Disclosure of Potential Conflicts of Interest

No potential conflicts of interest were disclosed.

Authors' Contributions

Conception and design: K. Pal, S. Bhattacharya, D. Mukhopadhyay
Development of methodology: K. Pal, S. Bhattacharya
Acquisition of data (provided animals, acquired and managed patients, provided facilities, etc.): K. Pal, Y. Cao, S.K. Dutta, E. Wang
Analysis and interpretation of data (e.g., statistical analysis, biostatistics, computational analysis): K. Pal, I.N. Gaisina, H. Gunosewoyo, D.D. Billadeau
Writing, review, and/or revision of the manuscript: K. Pal, I.N. Gaisina, H. Gunosewoyo, A.P. Kozikowski, D.D. Billadeau, D. Mukhopadhyay
Administrative, technical, or material support (i.e., reporting or organizing data, constructing databases): D. Mukhopadhyay
Study supervision: D. Mukhopadhyay

References

1. Siegel R, Naishadham D, Jemal A. Cancer statistics, 2012. CA Cancer J Clin 2012;62:10–29.
2. Bukowski RM. Natural history and therapy of metastatic renal cell carcinoma: the role of interleukin-2. Cancer. 1997;80:1198–220.
3. Bukowski RM. Cytokine therapy for metastatic renal cell carcinoma. Semin Urol Oncol. 2001;19:148–54.
4. Motzer RJ, Bukowski RM. Targeted therapy for metastatic renal cell carcinoma. J Clin Oncol 2006;24:5601–8.
5. Motzer RJ, Hutson TE, Tomczak P, Michaelson MD, Bukowski RM, Oudard S, et al. Overall survival and updated results for sunitinib compared with interferon alfa in patients with metastatic renal cell carcinoma. J Clin Oncol 2009;27:3584–90.
6. Motzer RJ, Molina AM. Targeting renal cell carcinoma. J Clin Oncol. 2009;27:3274–6.
7. Ljungberg B, Cowan NC, Hanbury DC, Hora M, Kuczyk MA, Merseburger AS, et al. EAU guidelines on renal cell carcinoma: the 2010 update. Eur Urol 2010;58:398–406.
8. Grunwald V, Kalanovic D, Merseburger AS. Management of sunitinib-related adverse events: an evidence- and expert-based consensus approach. World J Urol 2010;28:343–51.
9. Oya M, Ohtsubo M, Takayanagi A, Tachibana M, Shimizu N, Murai M. Constitutive activation of nuclear factor-kappa B prevents TRAIL-induced apoptosis in renal cancer cells. Oncogene 2001;20:3888–96.
10. Oya M, Takayanagi A, Horiguchi A, Mizuno R, Ohtsubo M, Marumo K, et al. Increased nuclear factor-kappa B activation is related to the tumor development of renal cell carcinoma. Carcinogenesis 2003;24: 377–84.
11. An J, Sun Y, Fisher M, Rettig MB. Maximal apoptosis of renal cell carcinoma by the proteasome inhibitor bortezomib is nuclear factor-kappa B dependent. Mol Cancer Ther 2004;3:727–36.
12. Hoeflich KP, Luo J, Rubie EA, Tsao MS, Jin O, Woodgett JR. Requirement for glycogen synthase kinase-3beta in cell survival and NF-kappa B activation. Nature 2000;406:86–90.
13. Ougolkov AV, Fernandez-Zapico ME, Savoy DN, Urrutia RA, Billadeau DD. Glycogen synthase kinase-3beta participates in nuclear factor kappaB-mediated gene transcription and cell survival in pancreatic cancer cells. Cancer Res 2005;65:2076–81.
14. Ougolkov AV, Bone ND, Fernandez-Zapico ME, Kay NE, Billadeau DD. Inhibition of glycogen synthase kinase-3 activity leads to epigenetic silencing of nuclear factor kappaB target genes and induction of apoptosis in chronic lymphocytic leukemia B cells. Blood 2007;110: 735–42.
15. Embi N, Rylatt DB, Cohen P. Glycogen synthase kinase-3 from rabbit skeletal muscle. Separation from cyclic-AMP-dependent protein kinase and phosphorylase kinase. Eur J Biochem 1980;107:519–27.
16. Parker PJ, Caudwell FB, Cohen P. Glycogen synthase from rabbit skeletal muscle; effect of insulin on the state of phosphorylation of the seven phosphoserine residues *in vivo*. Eur J Biochem 1983;130: 227–34.
17. Woodgett JR. Molecular cloning and expression of glycogen synthase kinase-3/factor A. Embo J 1990;9:2431–8.
18. Frame S, Cohen P. GSK3 takes centre stage more than 20 years after its discovery. Biochem J 2001;359:1–16.
19. Woodgett JR. Judging a protein by more than its name: GSK-3. Sci STKE 2001;2001:re12.
20. Dorn GWII, Force T. Protein kinase cascades in the regulation of cardiac hypertrophy. J Clin Invest 2005;115:527–37.
21. Doble BW, Woodgett JR. GSK-3: tricks of the trade for a multi-tasking kinase. J Cell Sci 2003;116:1175–86.
22. Force T, Woodgett JR. Unique and overlapping functions of GSK-3 isoforms in cell differentiation and proliferation and cardiovascular development. J Biol Chem 2009;284:9643–7.
23. Xu C, Kim NG, Gumbiner BM. Regulation of protein stability by GSK3 mediated phosphorylation. Cell Cycle 2009;8:4032–9.
24. Kaidanovich-Beilin O, Woodgett JR. GSK-3: functional insights from cell biology and animal models. Front Mol Neurosci 2011;4:40.
25. Cheng H, Woodgett J, Maamari M, Force T. Targeting GSK-3 family members in the heart: a very sharp double-edged sword. J Mol Cell Cardiol 2011;51:607–13.
26. Luo J. Glycogen synthase kinase 3beta (GSK3beta) in tumorigenesis and cancer chemotherapy. Cancer Lett 2009;273:194–200.
27. Jope RS, Yuskaitis CJ, Beurel E. Glycogen synthase kinase-3 (GSK3): inflammation, diseases, and therapeutics. Neurochem Res 2007;32: 577–95.
28. Kotliarova S, Pastorino S, Kovell LC, Kotliarov Y, Song H, Zhang W, et al. Glycogen synthase kinase-3 inhibition induces glioma cell death through c-MYC, nuclear factor-kappaB, and glucose regulation. Cancer Res 2008;68:6643–51.
29. Tan J, Zhuang L, Leong HS, Iyer NG, Liu ET, Yu Q. Pharmacologic modulation of glycogen synthase kinase-3beta promotes p53-dependent apoptosis through a direct Bax-mediated mitochondrial pathway in colorectal cancer cells. Cancer Res 2005;65: 9012–20.
30. Bilim V, Ougolkov A, Yuuki K, Naito S, Kawazoe H, Muto A, et al. Glycogen synthase kinase-3: a new therapeutic target in renal cell carcinoma. Br J Cancer 2009;101:2005–14.
31. Kim HM, Kim CS, Lee JH, Jang SJ, Hwang JJ, Ro S, et al. CG0009, a novel glycogen synthase kinase 3 inhibitor, induces cell death through cyclin D1 depletion in breast cancer cells. PLoS ONE 2013; 8:e60383.
32. Gaisina IN, Gallier F, Ougolkov AV, Kim KH, Kurome T, Guo S, et al. From a natural product lead to the identification of potent and selective benzofuran-3-yl-(indol-3-yl)maleimides as glycogen synthase kinase 3beta inhibitors that suppress proliferation and survival of pancreatic cancer cells. J Med Chem 2009;52:1853–63.
33. Hilliard TS, Gaisina IN, Muehlbauer AG, Gaisin AM, Gallier F, Burdette JE. Glycogen synthase kinase 3beta inhibitors induce apoptosis in ovarian cancer cells and inhibit *in vivo* tumor growth. Anticancer Drugs 2011;22:978–85.
34. Zhou BP, Deng J, Xia W, Xu J, Li YM, Gunduz M, et al. Dual regulation of Snail by GSK-3beta-mediated phosphorylation in control of epithelial-mesenchymal transition. Nat Cell Biol 2004;6:931–40.
35. Bachelder RE, Yoon SO, Franci C, de Herreros AG, Mercurio AM. Glycogen synthase kinase-3 is an endogenous inhibitor of Snail transcription: implications for the epithelial-mesenchymal transition. J Cell Biol 2005;168:29–33.
36. Zheng H, Li W, Wang Y, Liu Z, Cai Y, Xie T, et al. Glycogen synthase kinase-3 beta regulates Snail and beta-catenin expression during Fas-induced epithelial-mesenchymal transition in gastrointestinal cancer. Eur J Cancer 2013;49:2734–46.
37. Kao SH, Wang WL, Chen CY, Chang YL, Wu YY, Wang YT, et al. GSK3beta controls epithelial-mesenchymal transition and tumor metastasis by CHIP-mediated degradation of Slug. Oncogene 2013 Jul 15. [Epub ahead of print].

38. Thedieck C, Kuczyk M, Klingel K, Steiert I, Muller CA, Klein G. Expression of Ksp-cadherin during kidney development and in renal cell carcinoma. Br J Cancer 2005;92:2010–7.

39. Li X, Zhang Z, Xin D, Chua CW, Wong YC, Leung SC, et al. Prognostic significance of Id-1 and its association with EGFR in renal cell cancer. Histopathology 2007;50:484–90.

40. Buller CL, Loberg RD, Fan MH, Zhu Q, Park JL, Vesely E, et al. A GSK-3/TSC2/mTOR pathway regulates glucose uptake and GLUT1 glucose transporter expression. Am J Physiol Cell Physiol 2008; 295:C836–43.

41. Suzuki T, Bridges D, Nakada D, Skiniotis G, Morrison SJ, Lin JD, et al. Inhibition of AMPK catabolic action by GSK3. Mol Cell 2013;50:407–19.

42. Gavilan E, Sanchez-Aguayo I, Daza P, Ruano D. GSK-3beta signaling determines autophagy activation in the breast tumor cell line MCF7 and inclusion formation in the non-tumor cell line MCF10A in response to proteasome inhibition. Cell Death Dis 2013;4:e572.

43. Zhai P, Sciarretta S, Galeotti J, Volpe M, Sadoshima J. Differential roles of GSK-3beta during myocardial ischemia and ischemia/reperfusion. Circ Res 2011;109:502–11.

44. Parr C, Carzaniga R, Gentleman SM, Van Leuven F, Walter J, Sastre M. Glycogen synthase kinase 3 inhibition promotes lysosomal biogenesis and autophagic degradation of the amyloid-beta precursor protein. Mol Cell Biol 2012;32:4410–8.

45. Zhou X, Zhou J, Li X, Guo C, Fang T, Chen Z. GSK-3beta inhibitors suppressed neuroinflammation in rat cortex by activating autophagy in ischemic brain injury. Biochem Biophys Res Commun 2011;411:271–5.

46. Zhou J, Freeman TA, Ahmad F, Shang X, Mangano E, Gao E, et al. GSK-3alpha is a central regulator of age-related pathologies in mice. J Clin Invest 2013;123:1821–32.

47. Yang J, Takahashi Y, Cheng E, Liu J, Terranova PF, Zhao B, et al. GSK-3beta promotes cell survival by modulating Bif-1-dependent autophagy and cell death. J Cell Sci 2010;123:861–70.

48. Lin SY, Li TY, Liu Q, Zhang C, Li X, Chen Y, et al. GSK3-TIP60-ULK1 signaling pathway links growth factor deprivation to autophagy. Science 2012;336:477–81.

49. Cancer Genome Atlas Research Network. Comprehensive molecular characterization of clear cell renal cell carcinoma. Nature 2013;499: 43–9.

50. Woodard J, Joshi S, Viollet B, Hay N, Platanias LC. AMPK as a therapeutic target in renal cell carcinoma. Cancer Biol Ther 2010;10: 1168–77.

AAGR American Association for Cancer Research

Molecular Cancer Therapeutics

Inhibition of GSK-3 Induces Differentiation and Impaired Glucose Metabolism in Renal Cancer

Krishnendu Pal, Ying Cao, Irina N. Gaisina, et al.

Updated version	Access the most recent version of this article at: doi:10.1158/1535-7163.MCT-13-0681

Cited articles	This article cites 49 articles, 18 of which you can access for free at: http://mct.aacrjournals.org/content/13/2/285.full.html#ref-list-1

E-mail alerts	Sign up to receive free email-alerts related to this article or journal.
Reprints and Subscriptions	To order reprints of this article or to subscribe to the journal, contact the AACR Publications Department at pubs@aacr.org.
Permissions	To request permission to re-use all or part of this article, contact the AACR Publications Department at permissions@aacr.org.